Determination of the Earth's pole tide Love number k_2 from observations of polar motion using an adaptive Kalman filter approach

F. Seitz,[1] S. Kirschner,[1] and D. Neubersch[2,3]

Received 7 March 2012; revised 23 July 2012; accepted 24 July 2012; published 7 September 2012.

[1] The geophysical interpretation of observed time series of Earth rotation parameters (ERP) is commonly based on numerical models that describe and balance variations of angular momentum in various subsystems of the Earth. Naturally, models are dependent on geometrical, rheological and physical parameters. Many of these are weakly determined from other models or observations. In our study we present an adaptive Kalman filter approach for the improvement of parameters of the dynamic Earth system model DyMEG which acts as a simulator of ERP. In particular we focus on the improvement of the pole tide Love number k_2. In the frame of a sensitivity analysis k_2 has been identified as one of the most crucial parameters of DyMEG since it directly influences the modeled Chandler oscillation. At the same time k_2 is one of the most uncertain parameters in the model. Our simulations with DyMEG cover a period of 60 years after which a steady state of k_2 is reached. The estimate for k_2, accounting for the anelastic response of the Earth's mantle and the ocean, is $0.3531 + 0.0030i$. We demonstrate that the application of the improved parameter k_2 in DyMEG leads to significantly better results for polar motion than the original value taken from the Conventions of the International Earth Rotation and Reference Systems Service (IERS).

Citation: Seitz, F., S. Kirschner, and D. Neubersch (2012), Determination of the Earth's pole tide Love number k_2 from observations of polar motion using an adaptive Kalman filter approach, *J. Geophys. Res.*, *117*, B09403, doi:10.1029/2012JB009296.

1. Introduction

[2] The rotation of the Earth and its temporal variations have been monitored for decades with very high accuracy by space geodetic and astrometric observation systems, such as Global Navigation Satellite Systems, Satellite Laser Ranging, and Very Long Baseline Interferometry. Observations of the position of the Earth axis with respect to an Earth-fixed reference system and the angular velocity of the rotation are transformed into time series of the so-called Earth rotation parameters (ERP) polar motion and length-of-day (LOD) respectively.

[3] Precise knowledge of temporal variations of ERP is fundamental for a variety of applications, e.g., for the realization of highly precise time systems and geodetic reference systems, in order to relate Earth-fixed and space-fixed coordinate systems, and for precise navigation on Earth and in space. Besides, time series of ERP are of great interest for various disciplines of geosciences since dynamic processes in the Earth system are reflected in their temporal variations. In particular Earth rotation is influenced by the redistribution and motion of masses, involving the exchange of angular momentum between the Earth's subsystems, such as atmosphere, hydrosphere, and solid Earth [e.g., *Brzezinski et al.*, 2002; *Chao et al.*, 2000; *Chao and Yan*, 2010; *Dehant and de Viron*, 2002; *Eubanks*, 1993; *Greiner-Mai et al.*, 2003; *Gross et al.*, 2003]. Hence, the analysis of ERP time series allows for conclusions with respect to processes and interactions in the Earth system on various temporal scales.

[4] Since ERP are integrated quantities their variations are influenced by a multitude of effects in various subsystems of the Earth. Therefore the time series do not allow for conclusions with respect to particular processes without additional information from other observation techniques and numerical models. Some components of the ERP time series can be explained very well by models of specific Earth system processes, such as models for the effects of solid Earth and ocean tides [e.g., *Petit and Luzum*, 2010]. However, a comprehensive analysis of ERP time series over a wide spectral range requires a combined analysis and balance of a

[1]Earth Oriented Space Science and Technology, Technische Universität München, Munich, Germany.
[2]International Max Planck Research School on Earth System Modeling, Hamburg, Germany.
[3]Research Unit Sustainability and Global Change, Hamburg University, Hamburg, Germany.

Corresponding author: F. Seitz, Earth Oriented Space Science and Technology, Technische Universität München, D-80333 Munich, Germany. (seitz@bv.tum.de)

0148-0227/12/2012JB009296

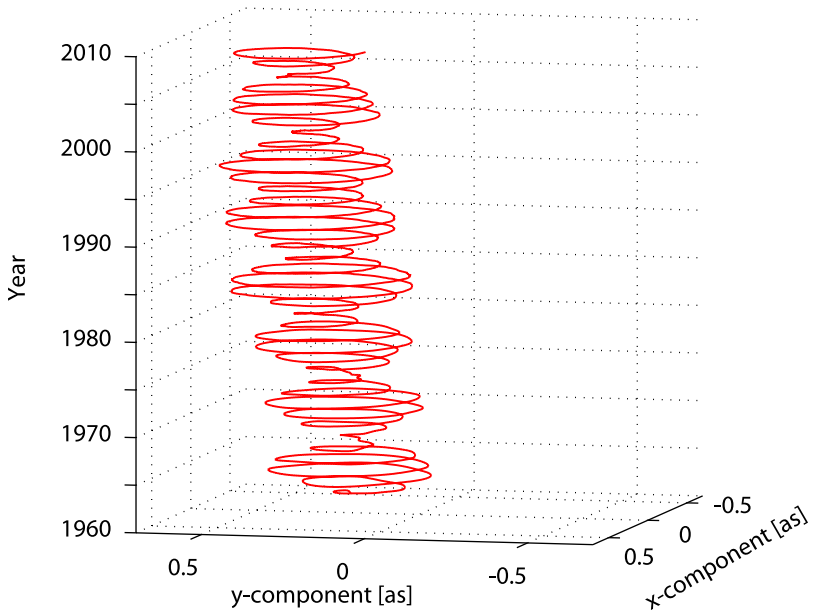

Figure 1. Observed polar motion (1962–2010) from the C04 series of the IERS [*Dick and Richter*, 2009].

multitude of Earth system processes. Therefore much effort is put into the development of extensive Earth system models in which the processes and interactions (e.g. exchange processes of energy, mass and momentum) within and between various subsystems of the Earth are described and balanced in a physically consistent way [e.g., *Gent et al.*, 2011]. Some of these models allow for the simulation and for an advanced analysis of the Earth's rotational dynamics over multiple temporal scales [*Hense et al.*, 2009; *Landerer et al.*, 2007; *Ponte et al.*, 2002; *Seitz and Drewes*, 2009].

[5] Such models are dependent on a variety of geometrical, rheological and physical parameters. Many of them are weakly determined with unknown accuracy from (simplified) model assumptions and can adulterate the model results. In this paper we report on the development of an inverse model approach with the objective of estimating and improving inaccurate model parameters using geodetic observations of ERP as constraints. Our study is based on the dynamic Earth system model DyMEG (Dynamic Model for Earth Rotation and Gravity [*Seitz et al.*, 2004]) on which an adaptive Kalman filter is applied. After a review of DyMEG (Section 2) we demonstrate the adaptive Kalman filter approach theoretically (Section 3) before we present numerical results (Section 4). Discussion and outlook conclude the paper (Section 5). In this article we focus on the estimation of an appropriate value for the pole tide Love number k_2. This parameter has earlier been identified as one of the most crucial model parameters of DyMEG since it directly influences the model's rotational dynamics [*Seitz and Kutterer*, 2005].

2. Physical Model of Earth Rotation

2.1. Theory

[6] Physical model approaches for Earth rotation are based on the balance of angular momentum in the Earth system. With respect to an Earth-fixed coordinate system the balance of angular momentum is described by the Euler-Liouville equation [*Lambeck*, 1980]:

$$\frac{d}{dt}H(t) + \omega(t) \times H(t) = L(t), \tag{1}$$

where $H(t)$ is the Earth's angular momentum vector, $L(t)$ denotes external torques due to, e.g., lunisolar gravitational forces and $\omega(t)$ is the Earth rotation vector. The angular momentum vector of the Earth comprising its deformable body and the fluid system components can be written as $H(t) = \mathbf{I}(t) \cdot \omega(t) + h(t)$. Here $\mathbf{I}(t)$ is the Earth's tensor of inertia that describes the time-variable distribution of the mass elements in the Earth system and $h(t)$ stands for angular momentum variations due to the motion of masses with respect to the reference system. The Earth rotation vector reads $\omega(t) = \Omega[m_1, m_2, 1 + m_3]^T$, where the small quantities m_i ($i = 1, 2, 3$; $m_i \ll 1$) describe deviations from the uniform rotation of the reference system with angular velocity $\Omega = 2\pi/86164$ s about its z-axis. The equatorial components m_1 and m_2 describe the time-variable orientation of the Earth rotation axis with respect to the z-axis of the reference system, and the absolute value of the Earth rotation vector is linked to the angular velocity of the rotation from which changes of LOD can be inferred. Variations of LOD will not be discussed in this article. Here we focus on the equatorial components that are directly related to polar motion. See *Gross* [1992] for details.

[7] Observations of polar motion (Figure 1) show a clear beat between two oscillations, namely an oscillation with a period of one year (approx. mean amplitude: 0.09 as; here as means seconds of arc), and another one with a period of about 432 days, the so-called Chandler oscillation (approx. mean amplitude: 0.17 as). The annual oscillation is predominantly induced by geophysical processes in the Earth system. The Chandler oscillation is a free rotational mode of the Earth, originating from the misalignment of the polar

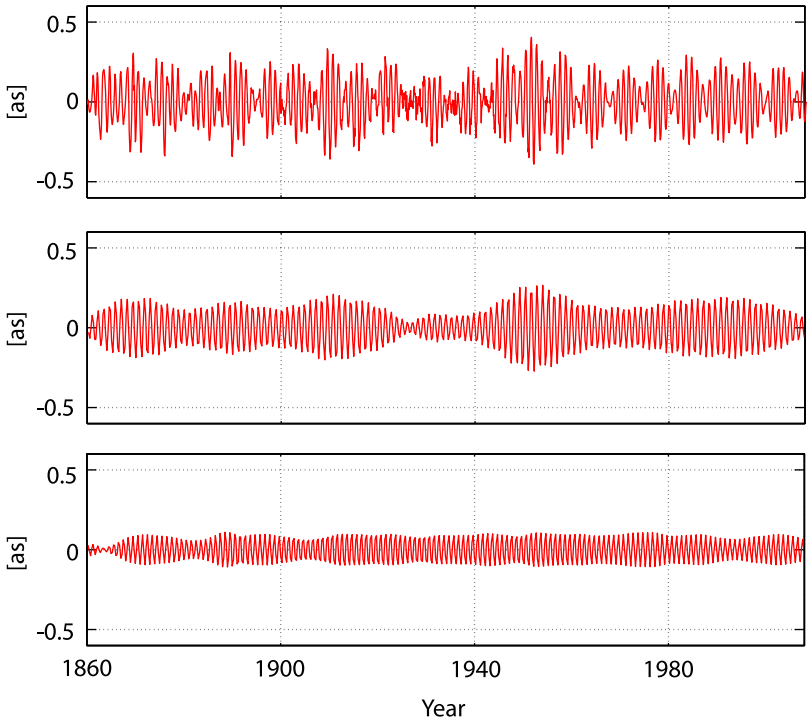

Figure 2. Decomposition of the *x*-component of polar motion from the C01/C04 series of the (top; trend removed) IERS into (middle) Chandler and (bottom) annual oscillation by means of wavelet filtering.

principal axis of inertia and the Earth rotation axis. Figure 2 displays time series of the two main signal components of polar motion for a period of 150 years between 1860 and 2010 from Morlet wavelet filtering [*Seitz and Schmidt*, 2005] of observations provided by the IERS in its C01 and C04 series [*Dick and Richter*, 2009]. While the annual signal is rather uniform, the Chandler oscillation features strong amplitude variations. Due to energy dissipation in the Earth system, mainly caused by the anelasticity of the Earth's mantle, the Chandler oscillation is damped. Angular momentum variations within the coupled atmosphere-ocean system excite this resonance oscillation and thus counteract its damping [*Gross*, 2000; *Seitz and Schmidt*, 2005].

2.2. Dynamic Earth System Model DyMEG

[8] Mass redistributions and motions in the components of the Earth system contribute to variations of the tensor of inertia $\mathbf{I}(t)$ and angular momenta $h(t)$ respectively. Thus they influence the balance of angular momentum and give rise to variations of Earth rotation. The effects from various subsystems are modeled and balanced within the dynamic Earth system model DyMEG. Figure 3 displays a principle sketch of the model; for more details on set-up and numerical implementation we refer the reader to the model description by *Seitz et al.* [2004]. DyMEG allows for the consideration and superposition of various effects which makes the model an ideal tool for the forward simulation and analysis of ERP.

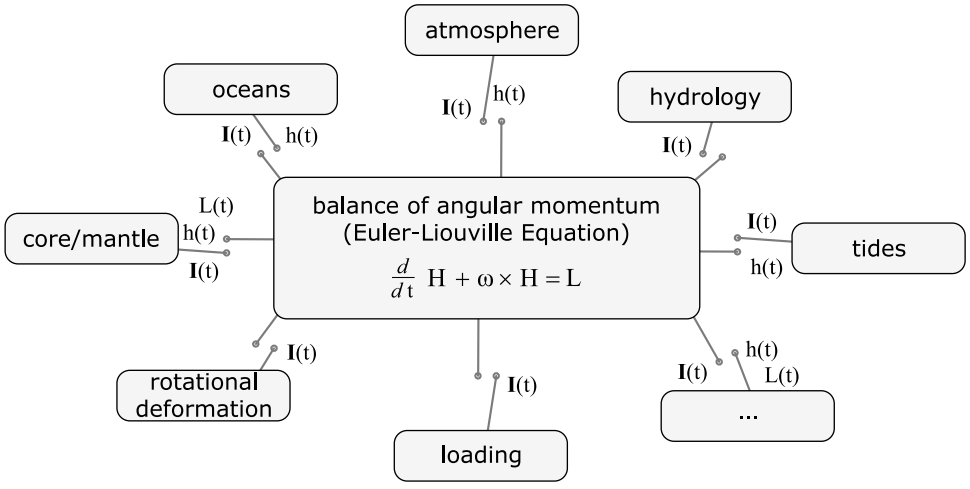

Figure 3. Principle sketch of DyMEG.

It has been shown in several studies that the results of DyMEG agree well with observed ERP on timescales from days to several years [e.g., *Seitz and Schmidt*, 2005].

[9] However, it has also been shown that the model results of DyMEG are highly dependent on the numerical values of some geometrical, rheological and physical model parameters. A sensitivity analysis of DyMEG [*Seitz and Kutterer*, 2005] revealed that especially the pole tide Love number k_2 is a critical parameter. It describes the back-coupling effect of polar motion on the mass distribution in the Earth system (so-called rotational deformations) as a consequence of the Earth's non-rigidity. The parameter k_2 depends on the rheological behavior of the Earth in response to polar motion that includes the previously mentioned dissipation due to friction (and therewith the damping of the Chandler oscillation). Consequently an erroneous value of k_2 directly entails a mismodeling of the Chandler oscillation.

[10] For our study we apply a simple Earth model that consists of an anelastic mantle and a spherical liquid core. Mantle and core are assumed to be fully decoupled, meaning that no exchange of angular momentum between these two model components is taken into account (see *Seitz et al.* [2004] for more details). For basic considerations on the applicability of such a model for studies related to Earth rotation we refer to, e.g., *Brzezinski* [2001] and *Moritz and Mueller* [1987]. A discussion of the effect of core-mantle decoupling on the parameter k_2 and the Chandler oscillation can be found, e.g., in the publications by *Dickman* [2005] and *Smith and Dahlen* [1981].

2.3. Rotational Deformations

[11] Rotational deformations are modeled as temporal variations of the Earth's centrifugal potential [*Petit and Luzum*, 2010]:

$$\begin{aligned}\Delta C_{21}(t) &= -\frac{\Omega^2 a^3}{3GM}(\Re(k_2)\cdot m_1(t) + \Im(k_2)\cdot m_2(t)) \\ \Delta S_{21}(t) &= -\frac{\Omega^2 a^3}{3GM}(\Re(k_2)\cdot m_2(t) - \Im(k_2)\cdot m_1(t)),\end{aligned} \tag{2}$$

(here higher order terms are neglected) where a and M denote radius and mass of the Earth and G is the gravitational constant. The response of the solid Earth and the ocean to variations of the Earth's centrifugal potential as a consequence of perturbations of the rotation axis is referred to as solid Earth pole tide and ocean pole tide respectively [*Smith and Dahlen*, 1981]. Variations of the geopotential coefficients depend on the rheological properties of the Earth and the ocean that are described by the complex valued pole tide Love number k_2. $\Re$ and $\Im$ stand for real and imaginary part respectively. The Conventions of the IERS [*Petit and Luzum*, 2010] provide a value of $k_2 = 0.3077 + 0.0036i$ ($i = \sqrt{-1}$) which accounts for solid Earth pole tides including the anelastic response of the Earth's mantle. The latter effect entails the damping of the Chandler oscillation. The provided value has been derived from theoretical model assumptions based on the geophysical standard Earth model PREM [*Dziewonski and Anderson*, 1981]. Since PREM is a substantially simplified representation of the real Earth, the accuracy of this value can not be quantified. The contribution of equilibrium ocean pole tides is incorporated by adding a surcharge of 0.044 [*Smith and Dahlen*, 1981; *Mathews et al.*, 2002]. Consequently the effective pole tide Love number k_2 equals $0.3517 + 0.0036i$. The assumption of equilibrium ocean pole tides means a simplification: Strictly speaking, the ocean pole tide involves a small dynamic component that might be capable of influencing the Chandler period by almost one day and also might contribute to the dissipation of energy and thus to the damping [*Dickman*, 1993]. In this respect the previously described formalism means an approximation, neglecting the small contributions of pole tide currents to relative angular momentum and changes in the tensor of inertia due to variations of the potential coefficients ΔC_{21} and ΔS_{21} that are dependent not only on polar motion (m_1, m_2) but also on polar motion rates ($\dot{m}_1, \dot{m}_2$). Alternative to the correction of the solid Earth pole tide Love number by adding 0.044, the effects of equilibrium ocean pole tides can be computed on the basis of a self-consistent equilibrium model following *Desai* [2002]. This approach is proposed by the most recent version of the IERS Conventions 2010 [*Petit and Luzum*, 2010], while it was not included in the previously effective IERS Conventions 2003 [*McCarthy and Petit*, 2004]. In this concept, variations of the potential coefficients ΔC_{21} and ΔS_{21} due to polar motion are computed separately for solid Earth pole tides (using the solid Earth pole tide Love number given above) and for ocean pole tides (using spherical harmonic coefficients from the equilibrium model). In our study we follow the previous approach by incorporating one pole tide Love k_2 number that accounts for both effects. However, we point out that our result is not directly comparable to numerical values of the alternative separated pole tide modeling approach due to conceptual differences (cf. Section 5). The changes of the Earth's centrifugal potential are directly linked to variations of the tensor of inertia:

$$\mathbf{I}_R(t) = \begin{pmatrix} 0 & 0 & \beta(\Re(k_2)\cdot m_1(t) + \Im(k_2)\cdot m_2(t)) \\ & 0 & \beta(\Re(k_2)\cdot m_2(t) - \Im(k_2)\cdot m_1(t)) \\ sym. & & 0 \end{pmatrix}, \tag{3}$$

with $\beta = \frac{\Omega^2 a^5}{3G}$ [*Lambeck*, 1980]. This way rotational deformations influence the balance of angular momentum and therewith the model results of DyMEG. In the previously mentioned sensitivity analysis of DyMEG the dependence of the model results of polar motion on the value of k_2 has been studied [*Seitz and Kutterer*, 2005]. The real part of k_2 is strongly related to the period of the modeled Chandler oscillation [*Smith and Dahlen*, 1981]. Figure 4 displays the Chandler period from several runs of DyMEG in which $\Re(k_2)$ was altered between 0.31 and 0.38 while $\Im(k_2)$ was kept constant ($0.0036i$).

[12] The model runs that are presented in the following were forced by consistent atmospheric and oceanic data from the atmospheric reanalysis of the National Centers for Environmental Prediction (NCEP) [*Kalnay et al.*, 1996] and the global ocean circulation model ECCO [*Fukumori*, 2002] over a time span of 60 years (1950–2009). Furthermore the effects of solid Earth deformations due to tides and loading are considered.

[13] Mass variations in the continental hydrology contribute predominantly to seasonal variations of ERP [*Chen et al.*, 2000]. Their contribution to inter-annual polar motion

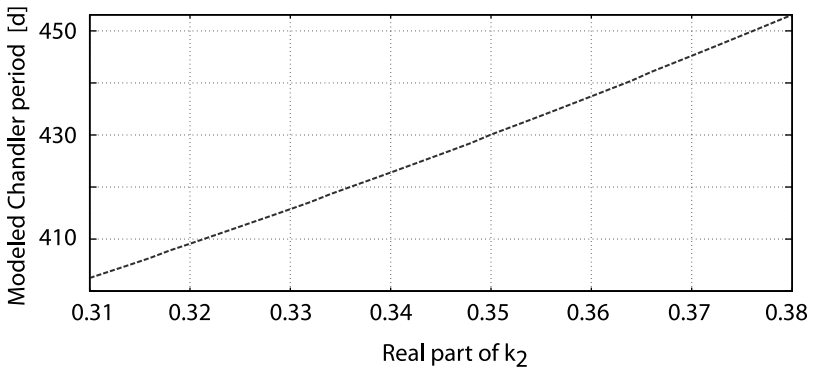

Figure 4. Modeled Chandler period from DyMEG against different values of $\Re(k_2)$. $\Im(k_2) = 0.0036$ is kept constant.

excitation is uncertain [*Chao and Yan*, 2010] and has been subject of several studies [e.g., *Brzezinski et al.*, 2012] that identified a considerable dependency of the result to the applied hydrological models. The strong sensitivity of polar motion excitation to any small error in a hydrological model follows from the distribution of continents and oceans on the Earth's surface and has been described in detail by *Chao and O'Connor* [1988]. Due to their small influence on the Chandler oscillation and their relatively large uncertainty hydrological mass variations are neglected in our study. Likewise, no interactions between core and mantle are considered in the applied model set-up. This includes the neglect of small mass redistributions in the core that might result from its response to polar motion.

[14] In order to study the effect of the imaginary part of k_2 on the model results, runs with DyMEG were performed in which $\Re(k_2)$ was kept constant (0.3517) while $\Im(k_2)$ was modified. Figures 5 and 6 show the results of two runs for $\Im(k_2) = 0.0020$ (weak damping) and $\Im(k_2) = 0.0045$ (strong damping) respectively. A clear influence of the imaginary part of k_2 on the damping of the Chandler oscillation is obvious: While both runs were started with identical initial conditions (i.e. pole coordinates), the Chandler amplitude becomes too high in the case of weak damping, while it develops too low in the case of strong damping.

[15] The damping of the Chandler oscillation is often expressed in terms of a quality factor Q. The quality factor is reciprocal to the specific dissipation of a damped oscillation. The specific dissipation of the modeled Chandler oscillation can be computed from model runs, in which geophysical excitations (i.e. atmosphere, oceans, tides and loading) are neglected. The envelopes of the resulting damped oscillations (Figure 7) can be expressed by $c(t) = c_0 \cdot e^{-\delta(t-t_0)}$, where c_0 is the initial amplitude of the oscillation and δ is the damping coefficient that is related to the specific dissipation (see *Seitz and Schuh* [2010] for details).

[16] From the two model runs with $\Im(k_2) = 0.0020$ and $\Im(k_2) = 0.0045$ we derive quality factors of $Q = 145$ and $Q = 65$ respectively. The value from the Conventions of the IERS corresponds to $Q = 82$.

[17] The quality factor of the observed Chandler oscillation has been discussed in various studies (Table 1). Its numerical value is characterized by a high level of uncertainty. In the following we propose a procedure for the

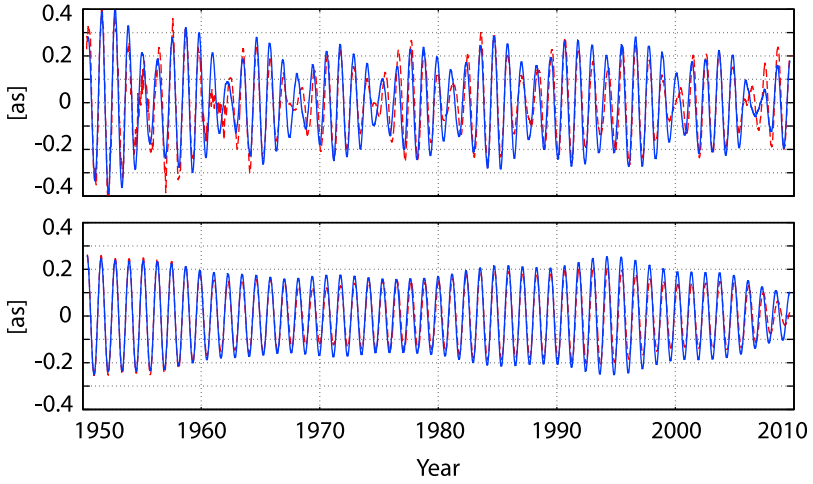

Figure 5. Model result for polar motion (x-component) from DyMEG with NCEP/ECCO forcing (blue), using $k_2 = 0.3517 + 0.0020i$ (weak damping). (top) Full signal; (bottom) Chandler oscillation. The red line shows the observed signal derived from the IERS C01/C01 series.

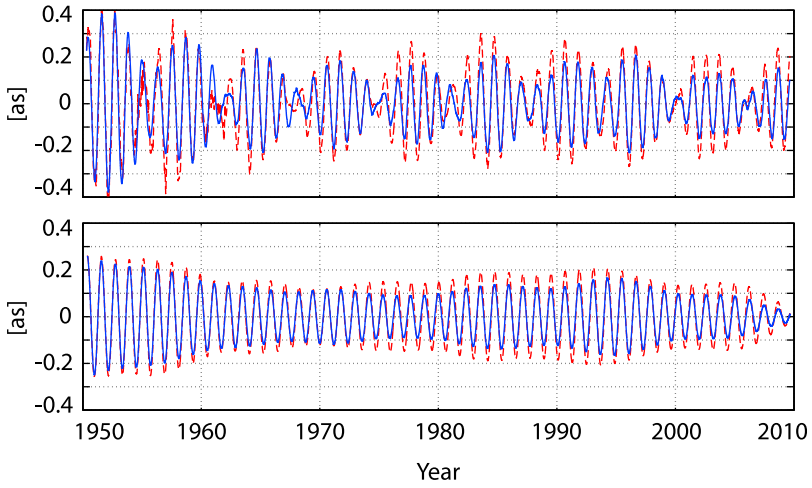

Figure 6. Same as Figure 5, using $k_2 = 0.3517 + 0.0045i$ (strong damping).

estimation of k_2 from the combination of observations with the dynamic Earth system model. Since k_2 is directly related to the Chandler oscillation of DyMEG an appropriate value for the parameter can be derived by inverting the model. Due to the high accuracy of the geodetic observations a significant improvement of k_2 can be expected. Note, that due to the neglect of interactions between core and mantle in DyMEG the resulting estimate for k_2 represents a mantle-ocean Love number [*Dickman*, 2005].

3. Adaptive Kalman Filter Approach

3.1. Theory of the Adaptive Kalman Filter

[18] The traditional Kalman filter is a discrete time filter. It is composed of a state-space system equation (model equation) and a measurement equation. The latter connects the system state (i.e. model predictions) to observations. In a recursive procedure an updated system state is estimated from a given previous state by combining model predictions with measurements. In this process the uncertainties of both the model predictions and the measurements are taken into account. A precondition of the applicability of a standard Kalman filter for meaningful state estimates is the availability of a system model with acceptable accuracy. In the problem at hand, the system model (DyMEG) contains inaccurate model parameters. Therefore we apply an *adaptive* Kalman filter (AKF) approach that allows for the adaptation of the system model in each step by adjusting the parameters in question (here: the Love number k_2) [*Neubersch*, 2010].

In the case of an AKF the system equation consists of two parts:

$$m_{k+1} = \mathbf{A}_k m_k + \mathbf{B}_k + w_k, \tag{4}$$

$$x^p_{k+1} = x^p_k, \tag{5}$$

where k is the time step index, m represents the system state (ERP), x^p is the vector of system parameters (real and imaginary part of the Love number k_2), w stands for the system noise (model accuracy), and $\mathbf{A}$ and $\mathbf{B}$ denote transition and input (forcing) matrix respectively. The two equations can be combined into

$$x_{k+1} = \mathbf{A}^a_k x_k + \mathbf{B}^a_k + w^a_k \tag{6}$$

with $x_k = (m_k, x^p_k)^T$, $\mathbf{A}^a_k = \begin{pmatrix} \mathbf{A}_k & 0 \\ 0 & \mathbf{E} \end{pmatrix}$, $\mathbf{B}^a_k = (\mathbf{B}_k, 0)^T$; $\mathbf{E}$ is a 2×2 identity matrix. The so-called extended state vector, the extended transition matrix and the extended input matrix are denoted by x, $\mathbf{A}^a$ and $\mathbf{B}^a$ respectively. Likewise the noise vector w is extended by $[\,0 \quad 0\,]^T$. The measurement equation reads

$$y_k = \mathbf{H} x_k + v_k, \tag{7}$$

where y are the geodetic observations (polar motion), v is the measurement noise and $\mathbf{H}$ is the so-called measurement

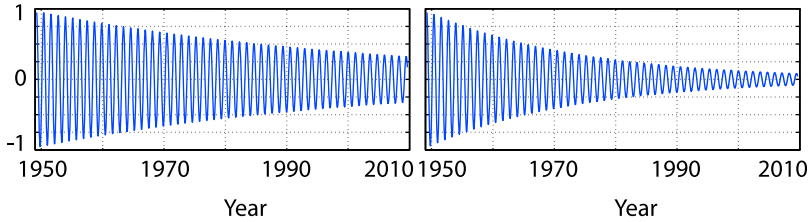

Figure 7. Damped Chandler oscillations from DyMEG (normalized) for (left) $\Im(k_2) = 0.0020$ and (right) $\Im(k_2) = 0.0045$.

Table 1. Quality Factors in the Literature

Q	Range	Source
100	[50, 400]	*Wilson and Haubrich* [1976]
24		*Lenhardt and Groten* [1985]
179	[47, >1000]	*Wilson and Vicente* [1990]
72	[30, 500]	*Kuehne et al.* [1996]
49	[35, 100]	*Furuya and Chao* [1996]
82		*Petit and Luzum* [2010]

matrix, selecting the polar motion components from the extended state vector x:

$$\mathbf{H} = \begin{pmatrix} 1 & 0 & 0 & 0 & 0 \\ 0 & 1 & 0 & 0 & 0 \end{pmatrix}. \tag{8}$$

3.2. From the Euler-Liouville Equation to the System Equation

[19] In Section 2.1 we introduced the Euler-Liouville equation on which the Earth system model DyMEG is based (note, that we omit the time-dependency (t) in the following derivations for the benefit of compactness):

$$\frac{d}{dt}(\mathbf{I}\ \omega + h) + \omega \times (\mathbf{I}\ \omega + h) = L. \tag{9}$$

In expanded form this equation reads:

$$\dot{\mathbf{I}}\ \omega + \mathbf{I}\ \dot{\omega} + \dot{h} + \omega \times \mathbf{I}\ \omega + \omega \times h = L. \tag{10}$$

We split the tensor of inertia into two parts:

$$\mathbf{I} = \mathbf{I}_G + \mathbf{I}_R. \tag{11}$$

[20] The first term $\mathbf{I}_G$ describes that part of the Earth's tensor of inertia that is independent from variations of the components m_1 and m_2 of the Earth rotation vector. Temporal variations of $\mathbf{I}_G$ result from geophysically induced mass redistributions in the solid Earth and the fluid system components. These are due to, e.g., atmospheric and oceanic mass variations as well as due to deformations by tides and loading. The second term $\mathbf{I}_R$ describes the effect of rotational deformations and depends on m_1 and m_2 (equation (3)). With all terms containing $\dot{m}_i$ (i = 1, 2, 3) assembled on the left hand side, the Euler-Liouville equation becomes [*Seitz and Schuh*, 2010]:

$$\dot{\mathbf{I}}_R\ \omega + \mathbf{I}\ \dot{\omega} = -\dot{\mathbf{I}}_G\ \omega - \omega \times \mathbf{I}\ \omega - \omega \times h + L - \dot{h}. \tag{12}$$

The left hand side of this equation reads in explicit form:

$$\begin{aligned} &\Omega\beta \begin{pmatrix} \Re(k_2)\dot{m}_1 + \Im(k_2)\dot{m}_2 \\ \Re(k_2)\dot{m}_2 - \Im(k_2)\dot{m}_1 \\ 0 \end{pmatrix} + \Omega\mathbf{I} \begin{pmatrix} \dot{m}_1 \\ \dot{m}_2 \\ \dot{m}_3 \end{pmatrix} = \\ &\left[\Omega\beta \begin{pmatrix} \Re(k_2) & \Im(k_2) & 0 \\ -\Im(k_2) & \Re(k_2) & 0 \\ 0 & 0 & 0 \end{pmatrix} + \Omega\mathbf{I} \right] \begin{pmatrix} \dot{m}_1 \\ \dot{m}_2 \\ \dot{m}_3 \end{pmatrix} =: \mathbf{F} \cdot \dot{m}. \end{aligned} \tag{13}$$

[21] Since the m_i are very small, all non-linear terms in m_i are dropped. On the right hand side we separate terms dependent on m_i from terms independent from m_i:

$$-\dot{\mathbf{I}}_G\ \omega - \omega \times \mathbf{I}\ \omega - \omega \times h + L - \dot{h} = \mathbf{N}' \cdot m + \mathbf{M}', \tag{14}$$

where $\mathbf{N}'$ and $\mathbf{M}'$ are matrices containing the respective variations of the tensor inertia, relative angular momenta and torques. Consequently we end up with the equation

$$\mathbf{F} \cdot \dot{m} = \mathbf{N}' \cdot m + \mathbf{M}', \tag{15}$$

or, by introducing $\mathbf{N} = \mathbf{F}^{-1} \cdot \mathbf{N}'$ and $\mathbf{M} = \mathbf{F}^{-1} \cdot \mathbf{M}'$:

$$\dot{m} = \mathbf{N} \cdot m + \mathbf{M}. \tag{16}$$

[22] From this reformulated Euler-Liouville equation the transition matrix $\mathbf{A}$ and the input matrix $\mathbf{B}$ of the Kalman system equation can be derived by discretization. It is assumed that $\mathbf{M}$ is invariant during one time step T (in our model we select T = 0.5 d). Consequently we can apply a zero-order hold discretization [*Chen and Francis*, 1995]:

$$\mathbf{A}_k = e^{\mathbf{N} \cdot T}, \qquad \mathbf{B}_k = \mathbf{N}^{-1}(\mathbf{A}_k - \mathbf{E}) \cdot \mathbf{M}. \tag{17}$$

[23] The model is initialized with ERP from geodetic observations at the starting date. As initial values for $\Re(k_2)$ and $\Im(k_2)$ we introduce 0.3517 and 0.0036 respectively. After a prediction step the modeled ERP are compared with geodetic observations. From this comparison a correction of the predicted values (the so-called Kalman gain) is derived. Simultaneously, improved values for the system parameters x^p (i.e. $\Re(k_2)$ and $\Im(k_2)$) are computed; see *Neubersch* [2010] for details.

4. Results

[24] Figure 8 shows the temporal development of the values for $\Re(k_2)$ and $\Im(k_2)$ over the entire time span of 60 years as derived from the AKF. While $\Re(k_2)$ reaches a steady state already after few years, $\Im(k_2)$ shows large fluctuations over many decades. However, by the end of the simulation the imaginary part converges to a stable estimate as well. The different behavior of real and imaginary part of the pole tide Love number is not surprising since $\Re(k_2)$ is directly related to the Chandler period that can be determined with high accuracy already after few years of the simulation. On the other hand, the damping of the Chandler oscillation is relatively low compared to the model time span, and the Chandler amplitude is largely influenced by the applied geophysical forcing. Therefore the estimates are characterized by a high degree of uncertainty at the beginning of the simulation, and a time span of several decades is required until the value reaches a steady state.

[25] By the end of our simulation we obtain a pole tide Love number $k_2 = 0.3531 + 0.0030i$. The standard deviation σ amounts to 0.0001 for both components. This value corresponds to a model Chandler period of 432.98 days and a quality factor of 97. The result for $\Re(k_2)$ agrees well with the initial value (difference: 0.4%), the result for $\Im(k_2)$ suggests

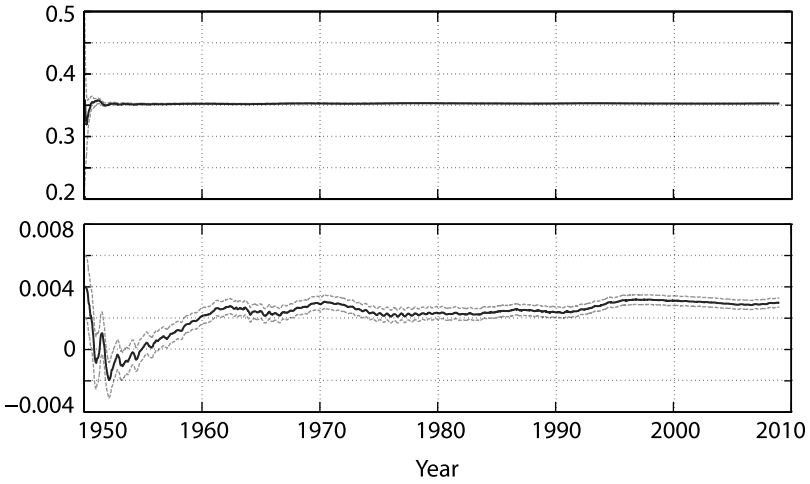

Figure 8. Result of the AKF (NCEP/ECCO forcing) for (top) $\Re(k_2)$ and (bottom) $\Im(k_2)$. Dotted lines indicate 2σ error margins.

a significantly lower damping than proposed by the initial value ($Q = 82$).

[26] In order to assess the improvement of the model we apply the estimated value of k_2 in DyMEG and run it as forward model. As above, we perform a simulation of the ERP over the entire time span of 60 years. The result (x-component) is displayed in Figure 9. The top panel shows the time series of the full polar motion, the lower panel shows the Chandler component. Both curves agree excellent with respective geodetic observations: the correlation coefficient for full polar motion is 0.95, the RMS difference amounts to 43.7 mas; for the Chandler oscillation the correlation coefficient is 0.99 and the RMS difference equals 17.3 mas.

[27] For comparison, Figure 10 shows the model results from DyMEG using the initial value for k_2. The amplitude of the oscillation clearly is too low toward the end of the simulation as a consequence of the strong damping. Correlation coefficients amount to 0.82 (full polar motion) and 0.89 (Chandler oscillation), the RMS differences are 82.2 mas and 55.7 mas respectively.

[28] In order to verify our result we repeat the estimation procedure with alternative forcing. The previously applied atmosphere/ocean model combination NCEP/ECCO is replaced by atmosphere and ocean data from ECMWF (European Centre for Medium-Range Weather Forecasts) and OMCT (Ocean Model for Circulation and Tides). Respective variations of $\mathbf{I}(t)$ and $h(t)$ were computed from ECMWF and OMCT effective angular momentum functions (see *Dobslaw et al.* [2010] for details).

[29] The ECMWF reanalysis ERA-40 [*Uppala et al.*, 2006] covers the period between 1958 and 2001. In order to be able to run our adaptive Kalman filter over a time span as long as possible (which has turned out to be decisive especially for a reliable estimate of $\Im(k_2)$; cf. Figure 8), we extended ERA40 after 2001 by operational ECMWF data until 2010. This way we created one time series that covers 52 years (hereafter simply called ECMWF). But it has to be

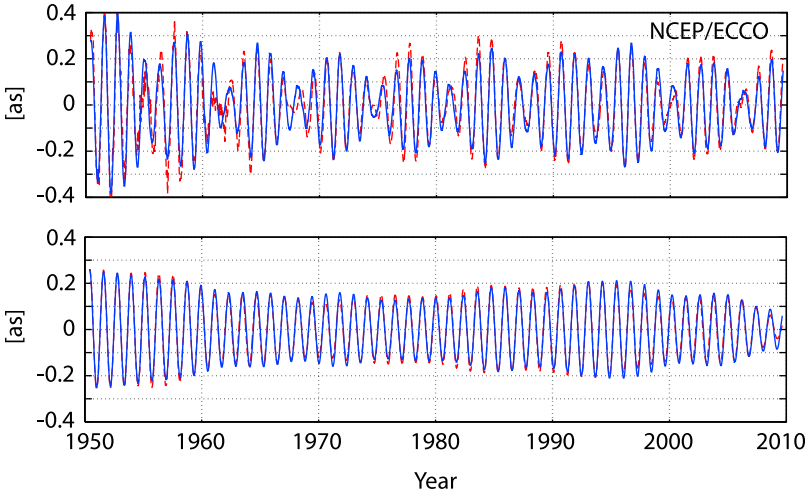

Figure 9. Model result for polar motion from DyMEG with NCEP/ECCO forcing (blue) applying the estimated value $k_2 = 0.3531 + 0.0030i$ (x-component). (top) Full polar motion; (bottom) Chandler component. Red: observed signals.

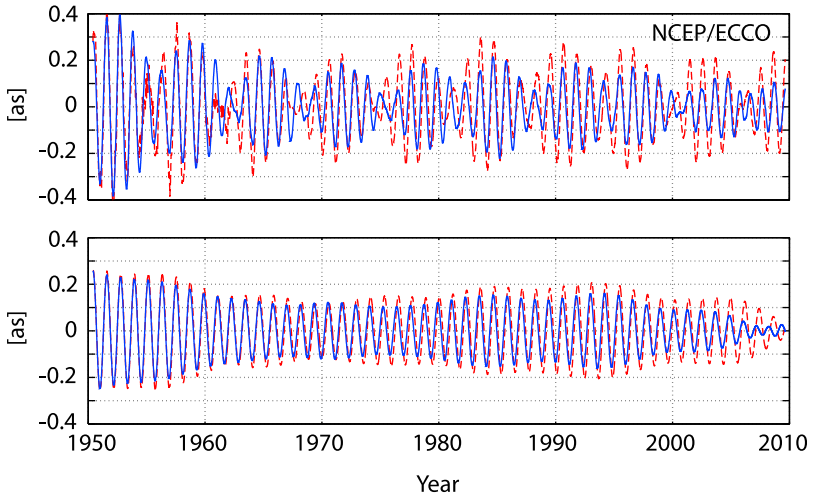

Figure 10. Same as Figure 9, using the initial value of the pole tide Love number $k_2 = 0.3517 + 0.0036i$.

kept in mind that this series is not fully consistent due to conceptual differences of the two data sets. Likewise a combined OMCT series was created by combining two OMCT versions forced by ERA40 and operational ECMWF data. The time span of 52 years is still significantly shorter than the period of 60 years covered by NCEP and ECCO. Therefore it is not possible to provide a result from our AKF that is fully comparable with the previous estimate of k_2, since it has been demonstrated above that including or excluding almost a decade of data might have a considerable effect on the numerical result.

[30] From this experiment (applying an unchanged set-up of the AKF) we obtain the value $k_2 = 0.3526 + 0.0025i$ (standard deviation: 0.0001 for both components), corresponding to a Chandler period of 432.07 days and a quality factor of 117. With this, the results for NCEP/ECCO and ECMWF/OMCT agree within the range of 3σ. Figure 11 shows the temporal development of the estimates for $\Re(k_2)$ and $\Im(k_2)$ in comparison with the results of the previous run using NCEP/ECCO. Like above the real part converges quickly. The imaginary part shows larger fluctuations over several decades, and by the end of the time series the convergence is not as good as in the case of NCEP/ECCO. Therefore this result for $\Im(k_2)$ appears to be less reliable.

[31] The result of a forward simulation from DyMEG with ECMWF/OMCT forcing (applying $k_2 = 0.3526 + 0.0025i$) is displayed in Figure 12. Like above the agreement between model simulation and geodetic observations (correlation coefficients: 0.91 (full polar motion) and 0.95 (Chandler oscillation); RMS differences: 53.2 mas and 36.6 mas respectively) improves with respect to a simulation using the initial value for k_2 (not shown; correlation coefficients: 0.88 (full polar motion) and 0.94 (Chandler oscillation); RMS differences: 61.0 mas and 42.3 mas respectively).

[32] However compared to NCEP/ECCO (Figure 9) the agreement of the DyMEG simulations with ECMWF/OMCT and the observations is significantly worse. A comparison of the Chandler components in the lower panels of

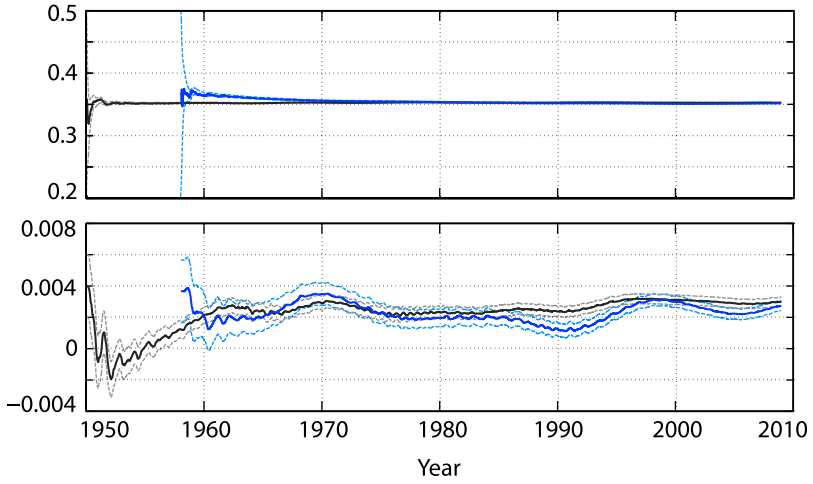

Figure 11. Comparison of the AKF results for NCEP/ECCO forcing (black; same curve as in Figure 8) and ECMWF/OMCT forcing (blue) for (top) $\Re(k_2)$ and (bottom) $\Im(k_2)$. Thin lines indicate 2σ error margins.

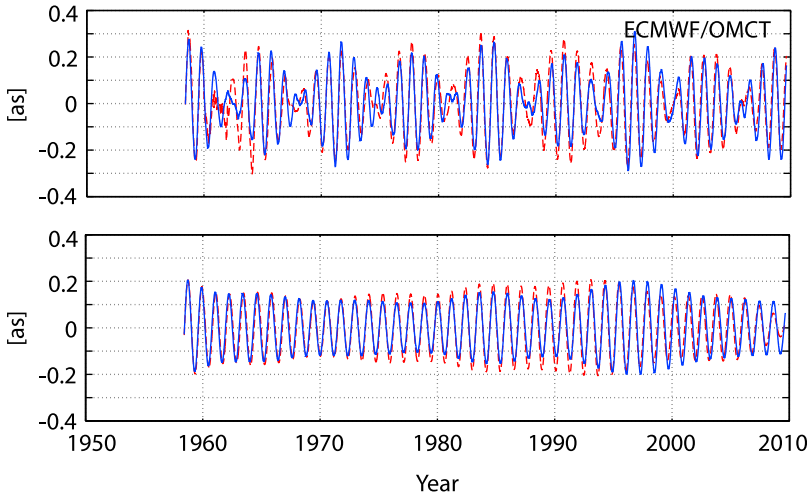

Figure 12. Model result for polar motion from DyMEG with ECMWF/OMCT forcing (blue) applying the estimated value $k_2 = 0.3526 + 0.0025i$ (x-component). (top) Full polar motion; (bottom) Chandler component. Red: observed signals.

Figures 9 and 12 reveals that NCEP/ECCO is superior with respect to the reproduction of the observed Chandler oscillation. This holds not only for the amplitude (which is influenced by the estimate of k_2) but also for the shape of the curve (which is independent from k_2 and depends on the excitation energy provided by the atmospheric and oceanic forcing). This leads to the conclusion that the atmospheric-oceanic variability in the Chandler frequency band described by NCEP/ECCO appears to be more realistic. Since the results for k_2 agree within the range of 3σ, the repetition of the experiment with the alternative forcing provides confidence on the procedure and the model set-up in general. But due to the length of the time series, the better convergence of the AKF, and the excellent agreement of the DyMEG result with the observations the value of $k_2 = 0.3531 + 0.0030i$ from NCEP/ECCO is more reliable.

5. Discussion

[33] The results of the previous section demonstrate the ability of the applied adaptive Kalman filter approach to improve the dynamic Earth system model DyMEG. We focused on the pole tide Love number k_2 for which the simulated polar motion is most sensitive. The real part of the parameter has earlier been determined with good accuracy, and our result (0.3531) is very close to the initial value (0.3517). The discrepancy of 0.4% between these values corresponds to a difference in the period of the modeled Chandler oscillation of less than one day. It might be possible that this discrepancy can at least partly be attributed to the neglect of the dynamic effect of the ocean pole tide in the equilibrium ocean pole tide correction of 0.044 to the solid Earth pole tide Love number (Section 2.3); see *Dickman* [1993] for a discussion. The result for the imaginary part (0.0030, corresponding to $Q = 97$) differs significantly from the initial value (0.0036, corresponding to $Q = 82$). Consequently DyMEG requires a lower damping than proposed by the value for the pole tide Love number provided by the Conventions of the IERS in combination with the (real valued) correction for the effect of equilibrium ocean pole tides following *Smith and Dahlen* [1981] and *Mathews et al.* [2002]. Up to now no runs have been performed with DyMEG using the alternative ocean pole tide model of *Desai* [2002] (cf. Section 2.3). As mentioned above this model follows a different concept for the computation of the effect of ocean pole tides. Therefore a different simulation result for polar motion can be expected. For testing purposes it is planned to implement this model in DyMEG. Before this has been realized we are unable to appraise if the result will be closer to the curve that we obtained from our adaptive Kalman procedure (Figure 9).

[34] The procedure (and therewith the estimated value of k_2) minimizes the discrepancy between the model result and the observations and thus depends on model set-up and forcing. With respect to the latter any over- or underestimation of the atmospheric-hydrospheric angular momentum variability in the Chandler frequency band might directly influence the estimate (the resulting imaginary part will be too large or too small respectively). For a discussion of a possible underestimation of atmospheric and oceanic angular momentum variations, in particular by NCEP and ECMWF, on intraseasonal, seasonal and inter-annual timescales see, e.g., *Chao and Yan* [2010] and the references therein. A further important task in this context is the evaluation of the system noise that is related to the accuracy of the models and data sets from which the forcing is derived.

[35] Although there are several tasks that require further investigation, the first results from the application of the adaptive Kalman filter that we presented in this paper are very promising. It has been demonstrated that observations of Earth rotation are important quantities for Earth system research that allow for the discovery of valuable new information via inverse model approaches. In principle the presented AKF approach can be extended to further parameters of the model. This, however, requires further studies concerning the sensitivity of the results on various model parameters and their correlations.

[36] **Acknowledgments.** This study was conducted in the frame of a project funded by DFG grant SE 1916/2-2 within the Research Unit FOR 584 Earth Rotation and Global Dynamic Processes. We thank Steven R. Dickman from the State University of New York, Binghamton, USA, and a second anonymous reviewer for their helpful comments on the manuscript. Time series of angular momentum variations for NCEP, ECCO, ECMWF, and OMCT were obtained from the Special Bureau for the Atmosphere and the Special Bureau for the Oceans in the frame of the IERS Global Geophysical Fluids Center.

References

Brzezinski, A. (2001), Diurnal and subdiurnal terms of nutation: A simple theoretical model for a nonrigid Earth, in *Proceedings of the Journées Systémes de Référence Spatio-temporels 2000*, edited by N. Capitaine, pp. 243–251, Obs. de Paris, Paris.

Brzezinski, A., C. Bizouard, and D. Petrov (2002), Influence of the atmosphere on Earth rotation: What new can be learned from the recent atmospheric angular momentum estimates?, *Surv. Geophys.*, *23*(1), 33–69, doi:10.1023/A:1014847319391.

Brzezinski, A., H. Dobslaw, R. Dill, and M. Thomas (2012), Geophysical excitation of the Chandler wobble revisited, in *Geodesy for Planet Earth*, *IAG Symp.*, vol. 136, edited by S. Kenyon et al., pp. 499–505, Springer, Berlin, doi:10.1007/978-3-642-20338-1_60.

Chao, B., and W. O'Connor (1988), Global surface water-induced seasonal variations in the Earth's rotation and gravitational field, *Geophys. J.*, *94*, 263–270, doi:10.1111/j.1365-246X.1988.tb05900.x.

Chao, B., and H. Yan (2010), Relation between length-of-day variation and angular momentum of geophysical fluids, *J. Geophys. Res.*, *115*, B10417, doi:10.1029/2009JB007024.

Chao, B., V. Dehant, R. Gross, R. Ray, D. Salstein, M. Watkins, and C. Wilson (2000), Space geodesy monitors mass transports in global geophysical fluids, *Eos Trans. AGU*, *81*, 247–250, doi:10.1029/00EO00172.

Chen, J., C. Wilson, B. Chao, C. K. Shum, and B. Tapley (2000), Hydrological and oceanic excitations to polar motion and length-of-day variation, *Geophys. J. Int.*, *141*, 149–156, doi:10.1046/j.1365-246X.2000.00069.x.

Chen, T., and B. Francis (1995), *Optimal Sampled-Data Control Systems*, Springer, London.

Dehant, V., and O. de Viron (2002), Earth rotation as an interdisciplinary topic shared by astronomers, geodesists and geophysicists, *Adv. Space. Res.*, *30*(2), 163–173, doi:10.1016/S0273-1177(02)00281-8.

Desai, S. (2002), Observing the pole tide with satellite altimetry, *J. Geophys. Res.*, *107*(C11), 3186, doi:10.1029/2001JC001224.

Dick, W., and B. Richter (Eds.) (2009), *IERS Annual Report 2007*, Bundesamt für Kartogr. und Geod., Frankfurt, Germany.

Dickman, S. R. (1993), Dynamic ocean tide effects on Earth's rotation, *Geophys. J. Int.*, *112*, 448–470, doi:10.1111/j.1365-246X.1993.tb01180.x.

Dickman, S. R. (2005), Rotationally consistent Love numbers, *Geophys. J. Int.*, *161*, 31–40, doi:10.1111/j.1365-246X.2005.02574.x.

Dobslaw, H., R. Dill, A. Groetzsch, A. Brzezinski, and M. Thomas (2010), Seasonal polar motion excitation from numerical models of atmosphere, ocean, and continental hydrosphere, *J. Geophys. Res.*, *115*, B10406, doi:10.1029/2009JB007127.

Dziewonski, A., and D. Anderson (1981), Preliminary Reference Earth model (PREM), *Phys. Earth Planet. Int.*, *25*, 297–356, doi:10.1016/0031-9201(81)90046-7.

Eubanks, T. (1993), Interactions between the atmosphere, oceans and crust: Possible oceanic signals in Earth rotation, *Adv. Space Res.*, *13*(11), 291–300, doi:10.1016/0273-1177(93)90231-Y.

Fukumori, I. (2002), A partitioned Kalman filter and smoother, *Mon. Weather Rev.*, *130*, 1370–1383, doi:10.1175/1520-0493(2002)130<1370:APKFAS>2.0.CO;2.

Furuya, M., and B. Chao (1996), Estimation of period and Q of the Chandler wobble, *Geophys. J. Int.*, *127*, 693–702, doi:10.1111/j.1365-246X.1996.tb04047.x.

Gent, P., et al. (2011), The Community Climate System Model version 4, *J. Clim.*, *24*, 4973–4991, doi:10.1175/2011JCLI4083.1.

Greiner-Mai, H., H., Jochmann, F. Barthelmes, and L. Ballani (2003), Possible influences of core processes on the Earth's rotation and the gravity field, *J. Geodyn.*, *36*, 343–358, doi:10.1016/S0264-3707(03)00054-1.

Gross, R. (1992), Correspondence between theory and observations of polar motion, *Geophys. J. Int.*, *109*, 162–170, doi:10.1111/j.1365-246X.1992.tb00086.x.

Gross, R. (2000), The excitation of the Chandler wobble, *Geophys. Res. Lett.*, *27*(15), 2329–2332, doi:10.1029/2000GL011450.

Gross, R., I. Fukumori, and D. Menemenlis (2003), Atmospheric and oceanic excitation of the Earth's wobbles during 1980–2000, *J. Geophys. Res.*, *108*(B8), 2370, doi:10.1029/2002JB002143.

Hense, A., et al. (2009), Physically consistent system model for the study of the Earth's rotation, surface deformation and gravity field parameters, *Rep. B 317*, German Geod. Comm., Munich.

Kalnay, E., et al. (1996), The NMC/NCAR 40-year reanalysis project, *Bull. Am. Meteorol. Soc.*, *77*, 437–471.

Kuehne, J., C. Wilson, and S. Johnson (1996), Estimates of the Chandler wobble frequency and Q, *J. Geophys. Res.*, *101*, 13,573–13,580, doi:10.1029/96JB00663.

Lambeck, K. (1980), *The Earth's Variable Rotation: Geophysical Causes and Consequences*, Cambridge Univ. Press, Cambridge, U. K.

Landerer, F., J. Jungclaus, and J. Marotzke (2007), Ocean bottom pressure changes lead to a decreasing length-of-day in a warming climate, *Geophys. Res. Lett.*, *34*, L06307, doi:10.1029/2006GL029106.

Lenhardt, H., and E. Groten (1985), Chandler wobble parameters from BIH and ILS data, *Manuscr. Geod.*, *10*, 296–305.

Mathews, P., T. Herring, and B. Buffet (2002), Modeling of nutation and precession: New nutation series for nonrigid Earth and insights into the Earth's interior, *J. Geophys. Res.*, *107*(B4), 2068, doi:10.1029/2001JB000390.

McCarthy, D., and G. Petit (Eds.) (2004), IERS Conventions (2003), *IERS Tech. Note 32*, Bundesamt für Kartogr. und Geod., Frankfurt, Germany.

Moritz, H., and I. I. Mueller (1987), *Earth Rotation*, Ungar, New York.

Neubersch, D. (2010), An adaptive Kalman filter approach for the estimation of the pole tide love number from observations of polar motion, MSc thesis D221, Inst. für Astron. und Phys. Geod., Tech. Univ. München, Munich, Germany.

Petit, G., and B. Luzum (Eds.) (2010), IERS Conventions (2010), *IERS Tech. Note 36*, Bundesamt für Kartogr. und Geod., Frankfurt, Germany.

Ponte, R., J. Rajamony, and J. Gregory (2002), Ocean angular momentum signals in a climate model and implications for Earth rotation, *Clim. Dyn.*, *19*(2), 181–190, doi:10.1007/s00382-001-0216-6.

Seitz, F., and H. Drewes (2009), Simulation of polar motion with a dynamic Earth system model over a period of 200 years (1860–2060), in *Proceedings of the Journées Systémes de Référence Spatio-temporels 2008*, edited by M. Soffeland N. Capitaine, pp. 123–126, Obs. de Paris, Paris.

Seitz, F., and H. Kutterer (2005), Sensitivity analysis of the non-linear Liouville equation, in *A Window on the Future of Geodesy*, *IAG Symp.* vol. 128, edited by F. Sanso, pp. 601–606, Springer, Berlin, doi:10.1007/3-540-27432-4_102.

Seitz, F., and M. Schmidt (2005), Atmospheric and oceanic contributions to Chandler wobble excitation determined by wavelet filtering, *J. Geophys. Res.*, *110*, B11406, doi:10.1029/2005JB003826.

Seitz, F., and H. Schuh (2010), Earth rotation, in *Sciences of Geodesy I: Advances and Future Directions*, edited by G. Xu, pp. 185–227, Springer, Berlin, doi:10.1007/978-3-642-11741-16.

Seitz, F., J. Stuck, and M. Thomas (2004), Consistent atmospheric and oceanic excitation of the Earth's free polar motion, *Geophys. J. Int.*, *157*(1), 25–35, doi:10.1111/j.1365-246X.2004.02208.x.

Smith, M., and F. Dahlen (1981), The period and Q of the Chandler wobble, *Geophys. J. R. Astron. Soc.*, *64*, 223–281, doi:10.1111/j.1365-246X.1981.tb02667.x.

Uppala, S., et al. (2006), The ERA-40 re-analysis, *Q. J. R. Meteorol. Soc.*, *131*, 2961–3012, doi:10.1256/qj.04.176.

Wilson, C., and R. Haubrich (1976), Meteorological excitation of the Earth's wobble, *Geophys. J. R. Astron. Soc.*, *46*, 707–743, doi:10.1111/j.1365-246X.1976.tb01254.x.

Wilson, C., and R. Vicente (1990), Maximum likelihood estimates of polar motion parameters, in *Variations of Earth Rotation*, *Geophys. Monogr. Ser.*, vol. 59, edited by D. McCarthy and W. Carther, pp. 151–155, AGU, Washington, D. C., doi:10.1029/GM059p0151.